Metabolomics (2025) 21:46
https://doi.org/10.1007/s11306-025-02249-9

ORIGINAL ARTICLE

Loss-of-functional mutation in *ANGUSTIFOLIA3* causes leucine hypersensitivity and hypoxia response during *Arabidopsis thaliana* seedling growth

Kensuke Kawade[1,2,3] · Mamoru Nozaki[3,9] · Gorou Horiguchi[4,5] · Tomoko Mori[6] · Katsushi Yamaguchi[6] · Mami Okamoto[2] · Hiromitsu Tabeta[2] · Shuji Shigenobu[6,7] · Masami Yokota Hirai[2] · Hirokazu Tsukaya[3,8]

Received: 3 September 2024 / Accepted: 25 March 2025 / Published online: 31 March 2025

Abstract

Introduction The *ANGUSTIFOLIA3* (*AN3*) gene encodes a transcriptional co-activator for cell proliferation in *Arabidopsis thaliana* leaves. We previously showed that *Physcomitrium patens AN3* orthologs promote gametophore shoot formation through arginine metabolism.

Objectives We analyzed the role of *AN3* in *Arabidopsis thaliana* to understand how seedling growth is regulated by metabolic and physiological modulations.

Methods We first explored amino acids that affect the seedling growth of *an3* mutants. Transcriptome and metabolome analyses were conducted to elucidate the metabolic and physiological roles of *AN3* during seedling growth. Lastly, we examined the distribution of reactive oxygen species to corroborate our omics-based findings.

Results Our results indicated that *an3* mutants were unable to establish seedlings when grown with leucine, but not arginine. Multi-omics analyses suggested that *an3* mutants exhibit a hypoxia-like response. Abnormal oxidative status was confirmed by detecting an altered distribution of reactive oxygen species in the roots of *an3* mutants.

Conclusion *AN3* helps maintain the leucine metabolism and oxidative balance during seedling growth in *Arabidopsis thaliana*. Future research is necessary to explore the interaction between these processes.

Keywords *ANGUSTIFOLIA3* · *Arabidopsis thaliana* · Hypoxia response · Leucine metabolism · Reactive oxygen species

Kensuke Kawade and Mamoru Nozaki have contributed equally to this work.

✉ Kensuke Kawade
kawade@mail.saitama-u.ac.jp

[1] Graduate School of Science and Engineering, Saitama University, Saitama City, Saitama 338-8570, Japan

[2] RIKEN Center for Sustainable Resource Science, Yokohama, Kanagawa 230-0045, Japan

[3] Exploratory Research Center on Life and Living Systems (ExCELLS), National Institutes of Natural Sciences, Okazaki, Aichi 444-8787, Japan

[4] College of Science, Rikkyo University, Toshima-ku, Tokyo 171-8501, Japan

[5] Research Center for Life Science, Rikkyo University, Toshima-ku, Tokyo 171-8501, Japan

[6] National Institutes of Natural Sciences, National Institute for Basic Biology, Okazaki, Aichi 444-8585, Japan

[7] School of Life Science, Graduate University for Advanced Studies (SOKENDAI), Okazaki, Aichi 444-8585, Japan

[8] Graduate School of Science, The University of Tokyo, Bunkyo-ku, Tokyo 113-0033, Japan

[9] Present address: Institute of Vegetable and Floriculture Science, National Agriculture and Food Research Organization (NARO), Tsu, Mie 514-2392, Japan

1 Introduction

Amino acids are used as materials for protein biosynthesis and as carbon backbones to produce various metabolites. Given their physiological and metabolic importance, their metabolism generally remains stable even under fluctuating environments. Accumulating evidence nevertheless suggests that some amino acid metabolisms are relevant to specific plant tissue growth, for example, L-arginine (Arg) metabolism in the moss leafy shoot-like tissue growth, L-threonine (Thr) metabolism in the hypocotyl elongation, γ-aminobutyric acid (GABA) shunt in leaf formation, and L-serine (Ser) metabolism in the liverwort sperm and embryo development (Kawade et al., 2020; Tabeta et al., 2022; Toyokura et al., 2011; Wang et al., 2024). Although the molecular mechanisms of this regulation remain largely unclear, amino acid metabolism presents a promising target for understanding how plant tissue growth is regulated through metabolic and physiological modulations (Kawade et al., 2023).

Leaf growth depends on the increase in the number and size of the constituent cells. As these two processes are promoted by cell proliferation and subsequent post-mitotic cell expansion, respectively, a series of studies explore the genetic mechanisms operating in cell proliferation and/or subsequent post-mitotic cell expansion. The *ANGUSTIFOLIA3* (*AN3*) gene encodes a transcriptional co-activator promoting cell proliferation in the leaves of the seed plant *Arabidopsis thaliana* (hereafter, Arabidopsis), one of the model organisms for plant research. The *an3* mutants exhibit fewer leaf cells, whereas the *AN3* overexpressors have more cells in the leaves compared to wild-type (WT) plants (Horiguchi et al., 2005; Kim & Kende, 2004). The transcription factor GROWTH-REGULATING FACTOR5 (GRF5) and SWITCH/SUCROSE NONFERMENTING (SWI/SNF) chromatin remodeling complexes have been identified as physical interaction partners of AN3, promoting cell proliferation in Arabidopsis leaves (Horiguchi et al., 2005; Hussain et al., 2022; Nelissen et al., 2015; Vercruyssen et al., 2014). Recent studies have shown that AN3 is important in iron uptake and response through its interaction with the transcription factor FER-LIKE IRON DEFICIENCY-INDUCED TRANSCRIPTION FACTOR (FIT) (Zheng et al., 2023). We previously demonstrated that Arg metabolism is compromised in the gametophore shoots, which consist of stems and leaves, of the moss *Physcomitrium patens an3* (*Ppan3*) mutants, leading to stunted shoot growth, similar to that observed in WT plants treated with Arg (Kawade et al., 2020). These findings suggest that *AN3* might be linked to metabolic and/or physiological conditions while directly regulating tissue growth and developmental processes.

We conducted amino acid screening to explore the relevance of amino acid metabolism in *AN3*-mediated regulations using Arabidopsis seedlings as a growth model. This experiment, along with our transcriptome and metabolome analyses, suggested that L-leucine (Leu) metabolism is compromised in *an3* mutants. We also observed that the *an3* mutants exhibit hypoxia-like transcriptional and metabolic responses as represented by the increase in the expression of *PYRUVATE DECARBOXYLASE 1* (*PDC1*) and *ALCOHOL DEHYDROGENASE 1* (*ADH1*) (Gibbs et al., 2011) and in the accumulation of L-phenylalanine (Phe), L-alanine (Ala), and GABA (Lothier et al., 2020; Miyashita & Good, 2008) associated with the altered distribution of reactive oxygen species (ROS). Based on these results, we propose that *AN3* helps to maintain Leu metabolism and oxidative status during seedling growth in Arabidopsis.

2 Materials and methods

2.1 Plant materials and culture conditions

We used the *Arabidopsis thaliana* (L.) Heynh Colombia-0 (Col-0) wild-type (WT) accession. The *an3-2* and *an3-4* mutants were isolated from X-ray-irradiated populations (Horiguchi et al., 2005). *MIR396A* genomic fragments were amplified using the primers, 5'-CACGGGGGACTC TAGTGCTGTAAAAGAATGACCCTTC-3′ and 5′- GAT CGGGGAAATTCGAAACTCATAGACAGAAGTTAGG G-3′, and introduced into XbaI/SacI-digested pSMAH621 using the In-Fusion HD Cloning Kit (Takara Bio Inc.). The resulting vector was used to transform Col-0 plants, obtaining a single insertion line of *Pro35S:MIR396A*. Transgenic lines constitutively expressing *KIP-RELATED PROTEIN 2* (*KRP2*) under the cauliflower mosaic virus *35 S* promoter (*Pro35S:KRP2*), *fugu2*, and *grf5* were described elsewhere (Ferjani et al., 2007; Horiguchi et al., 2005). Transgenic lines expressing *AN3* fused with *GREEN FLUORESCENT PROTEIN* (*AN3-GFP*) driven by a ~ 1.5 kb genomic fragment upstream of the *AN3* gene in the *an3-4* genetic background (*an3-4/ProAN3:AN3-GFP*) were previously established (Kawade et al., 2013). β-glucuronidase (GUS)-reporter lines using the *AN3* promoter fragment in the WT and *an3-4* genetic backgrounds (*ProAN3:GUS* and *an3-4/ProAN3:GUS*, respectively) were described elsewhere (Kawade et al., 2013). Seeds were sown on half-strength Murashige-Skoog (MS) medium (Murashige & Skoog, 1962) solidified with 0.2% (w/v) gellan gum and 1% (w/v) sucrose, containing each amino acid at the indicated concentrations (0, 0.5, 1.0, 3.0, or 6.0 mM). The seeds were stratified at 4 °C for 3 days in the dark, and then plants were cultured at 22 °C under a 16-h light (50 μmol m^{-2} s^{-1} from

white fluorescent lamps) and 8-h dark cycle for an additional 2 or 3 days for metabolite analysis and 6 or 7 days for morphological observation, otherwise noted.

2.2 RNA-sequencing

Thirty seedlings were collected in a microtube, frozen in liquid nitrogen, and stored at −80 °C prior to use. Total RNA was extracted from the frozen seedlings using the RNeasy Plant Mini Kit (Qiagen) with on-column DNase I digestion (Qiagen), following the manufacturer's instructions. RNA concentration and quality were evaluated using a Qubit fluorometer (Invitrogen) and Bioanalyzer 2100 (Agilent), respectively. RNA sequencing libraries were prepared using the TruSeq Stranded mRNA Sample Prep Kit (Illumina). Libraries were pooled and sequenced on the HiSeq 1500 platform in 66-bp single end mode (Illumina) in the NIBB Trans-Omics Facility. RNA sequencing raw reads were quality-controlled using Cutadapt v.1.11 (Martin, 2011) and mapped against the *Arabidopsis* TAIR10 reference genome using TopHat2 v.2.1.1 (Kim et al., 2013). Raw sequencing data are available via the DNA Data Bank of Japan (DDBJ) BioProject (PRJDB18188).

2.3 Bioinformatics analyses of transcriptome data

We used Cufflinks v.2.2.1 (Trapnell et al., 2010) to estimate differentially expressed genes (DEGs) in the *an3-4* mutants compared with WT plants, using a false discovery rate < 0.05 and fold change > 2 or < 0.05 as thresholds. Gene Ontology (GO) enrichment analysis of the DEGs was performed using PANTHER GO-Slim Biological Process v.15.0 (Mi et al., 2019). AtCAST v.3.1 (Kakei & Shimada, 2015) was used for similarity analysis of the transcriptome data. These analyses were performed using the default parameter settings.

2.4 Mass spectrometry-based metabolite analysis

Approximately 50 mg of the seedlings were collected in a microtube, frozen in liquid nitrogen, and stored at −80 °C until analysis. Seedling samples were homogenized using Multi-beads shocker (YASUI KIKAI).

For liquid chromatography coupled with tandem mass spectrometry (LC-MS/MS), metabolites were extracted using 80% (v/v) methanol with 0.1% (v/v) formic acid and an internal standard of 1 µM methionine sulfone. The supernatant was collected after centrifugation at 14,560 ×g for 3 min at 4 °C using METALFUGE MBG-312 C (YASUI KIKAI) and dried in a centrifugal concentrator. The residue was re-dissolved in 20 µL of 0.1% (v/v) formic acid and analyzed with a Triple TOF 5600 system (AB Sciex) connected to ACQUITY UPLC H-Class (Waters) as previously reported (Kawade et al., 2020) with the following conditions: column, Discovery HS F5-3 (3 µm) 2.1 × 150 mm (Discovery); solvents, water with 0.1% formic acid (A) and acetonitrile with 0.1% formic acid (B); gradient program, 50% B (0 min) and 95% B (15 min); flow rate, 100 µL/min; column temperature, 30 °C; injection volume, 2 µL; analysis mode, electrospray ionization with capillary voltage −4.5 kV for negative ion mode. Data were obtained in the multiple reaction monitoring (MRM) mode. The MRM transitions used in the analysis were summarized in Supplemental Table S1. The retention time of the targeted metabolites was determined using standard compounds. The targeted metabolites were normalized by methionine sulfone. The raw data of peak area values were collected and analyzed using MultiQuant™ 2.1 software (AB Sciex).

For gas chromatography-tandem mass spectrometry (GC-MS/MS)-based metabolome analysis, metabolites were extracted from seedlings grown on half-strength MS medium for 2 days under Leu-untreated conditions or 3 days under 1.0 mM Leu-treated conditions using 80% (v/v) methanol with 0.1% (v/v) formic acid and an internal standard of 12 µg/mL ribitol. After centrifugal concentration, the dried residue was dissolved in MOX reagent (2% methoxyamine-hydrogen chloride in pyridine) and incubated overnight at 37 °C in a thermomixer. *N*-Methyl-*N*-(trimethylsilyl)trifluoroacetamide (MSTFA) + 1% 2,2,2-trifluoro-*N*-methyl-*N*-trimethylsilylacetamide, chlorotrimethylsilane (TMCS) was added to the samples, followed by additional incubation at 37 °C for 30 min. The processed samples were analyzed with an AOC-5000 Plus with GCMS-TQ8040 instrument (Shimadzu) as previously described (Okamura et al., 2021) with the following conditions: column, BPX-5 (0.25 mm inner diameter, film thickness = 0.25 µm × 30 m) (SGE); insert, split insert with wool (RESTEK); carrier, helium gas in split mode (split ratio 1:30) at a flow rate of 40.4 mL/min; GC vaporization temperature, 250 °C; temperature gradient program, 60 to 330 °C at a rate of 15 °C/s; interface temperature of MS, 280 °C; ion source temperature of MS, 200 °C; loop time of data collection, 0.3 s. Data were obtained in the MRM mode. The MRM transitions used in the analysis were summarized in Supplemental Table S2. LabSolutions Insight (Shimadzu) was used to collect raw data and calculate their peak area values. Quality-filtered metabolites were selected with a signal-to-noise ratio > 5 and a relative standard deviation of quality control samples < 30%. Normalization of peak area values was conducted using LOWESS/Spline normalization tools (Tsugawa et al., 2014).

The metabolome data were transformed into $\log_2$-scaled values for volcano plots and calculated *z*-scores for principal component analysis (PCA). We performed data processing, analysis, and visualization using our customized scripts

written in MATLAB software (The MathWorks) with the aid of the function pca.

2.5 Microscopy

Superoxide (O_2^-) was detected using nitroblue tetrazolium (NBT) as previously described (Dunand et al., 2007). Seedlings were immersed in 20 mM phosphate buffer (pH 6.1) containing 2 mM NBT for 15 min, and then washed with distilled water. Hydrogen peroxide (H_2O_2) was detected using the fluorescent indicator BES-H_2O_2-Ac, as previously described (Tsukagoshi et al., 2010). Seedlings were immersed in 20 mM phosphate buffer (pH 6.8) containing 50 µM BES-H_2O_2-Ac for 30 min, and then washed with distilled water. Nitric oxide (NO) was detected using diaminofluorescein-2 diacetate (DAF-2 DA), as previously described (Kojima et al., 1998). Seedlings were immersed in 20 mM phosphate buffer (pH 6.8) containing 50 µM DAF-2 DA for 60 min, and then washed with distilled water. The WT and *an3-4* seedlings grown on half-strength MS medium for 2 days were used to detect superoxide (O_2^-), hydrogen peroxide (H_2O_2), and nitric oxide (NO).

GUS activity was visualized using a previously described method (Donnelly et al., 1999). Stained tissues were cleared in a chloral hydrate solution (200 g chloral hydrate, 20 g glycerol, and 50 mL distilled water) before observation.

Optical and fluorescence images were captured using a stereoscopic microscope (MZ16a; Leica Microsystems) and a confocal laser scanning microscope (A1Rsi; Nikon), respectively, as previously described (Kawade et al., 2018; Tomoi et al., 2020).

3 Results

3.1 Growth suppression of *an3* seedlings by leucine

We assessed the cotyledon area and primary root length of Arabidopsis WT plants and *an3* mutants treated with L-arginine (Arg) and other 19 proteinogenic amino acids to determine whether seedling growth is affected by amino acid treatment. We observed significant suppression of cotyledon expansion in the *an3* mutants compared with WT plants when treated with L-isoleucine (Ile), L-leucine (Leu), L-lysine (Lys), and L-valine (Val) (Fig. 1A). Primary root growth was also impaired in *an3* mutants under treatment with Ile, Leu, Lys, or Val (Fig. 1B). This suppressive effect was less pronounced in WT plants and *an3* mutants treated with Arg (Fig. 1A and B). As Ile, Leu, and Val are branched-chain amino acids (BCAAs) and growth suppression was most evident in Leu-treated *an3* mutants among the 20 amino acids, we explored the concentration dependency of BCAAs on growth suppression. Our tests showed a clear difference in seedling growth between WT plants and *an3* mutants under 1.0 mM Leu treatment, which was the same condition used in our screening (Fig. 1C).

Given the severe suppression of seedling growth by Leu, particularly in *an3* mutants, we next examined seedling establishment under Leu treatment. We found that although 84% of Leu-treated WT plants successfully established seedlings, as represented by expanding green cotyledons, 86–96% of *an3* mutants displayed immediate growth arrest after germination (Fig. 1D). To determine whether this growth suppression was caused by the functional disruption of *AN3* or a more generic effect related to cell proliferation defect, we studied seedling establishment in the *Pro35S:KRP2* transgenic lines and *fugu2* mutants, which are both known for their precocious exit from the mitotic cell cycle (De Veylder et al., 2001; Ferjani et al., 2007; Hisanaga et al., 2013; Verkest et al., 2005). Both *Pro35S:KRP2* and *fugu2* established seedlings with cotyledon expansion and greening similar to WT plants, even under Leu treatment (Fig. 1E). This result suggests that growth suppression by Leu is linked to the functional disruption of *AN3* rather than a general cell proliferation defect. We also investigated whether the *grf5* mutants and *Pro35S:MIR396A* transgenic lines, which are involved in the *AN3*-mediated regulation of cell proliferation, experience growth suppression by Leu (Horiguchi et al., 2005; Rodriguez et al., 2010). Both *grf5* mutants and *Pro35S:MIR396A* established seedlings comparable to the WT plants under Leu treatment (Fig. 1F), suggesting that the observed growth suppression by Leu is independent of the previously known genetic pathway for *AN3*-mediated regulation of cell proliferation.

3.2 Molecular signatures related to hypoxia in *an3* seedlings

We conducted a transcriptome analysis of WT and *an3* seedlings under both Leu-treated and untreated conditions using RNA sequencing to explore how *AN3* influences seedling growth. This analysis revealed that *an3* seedlings had 253 upregulated and 79 downregulated genes in the untreated condition, and 732 upregulated and 1348 downregulated genes in the Leu-treated condition, compared to WT plants. Genes potentially involved in the Leu degradation pathway (Angelovici et al., 2013; Schertl et al., 2017) were slightly but broadly downregulated in Leu-treated *an3* mutants, whereas they maintained relatively normal expression levels under the untreated condition (Fig. 2A). To assess whether the metabolic profile of the Leu degradation pathway was affected in Leu-treated *an3* seedlings, we measured accumulated degradation intermediates of Leu using LC-MS/MS. We found that the levels of 4-methyl-2-oxovaleric acid,

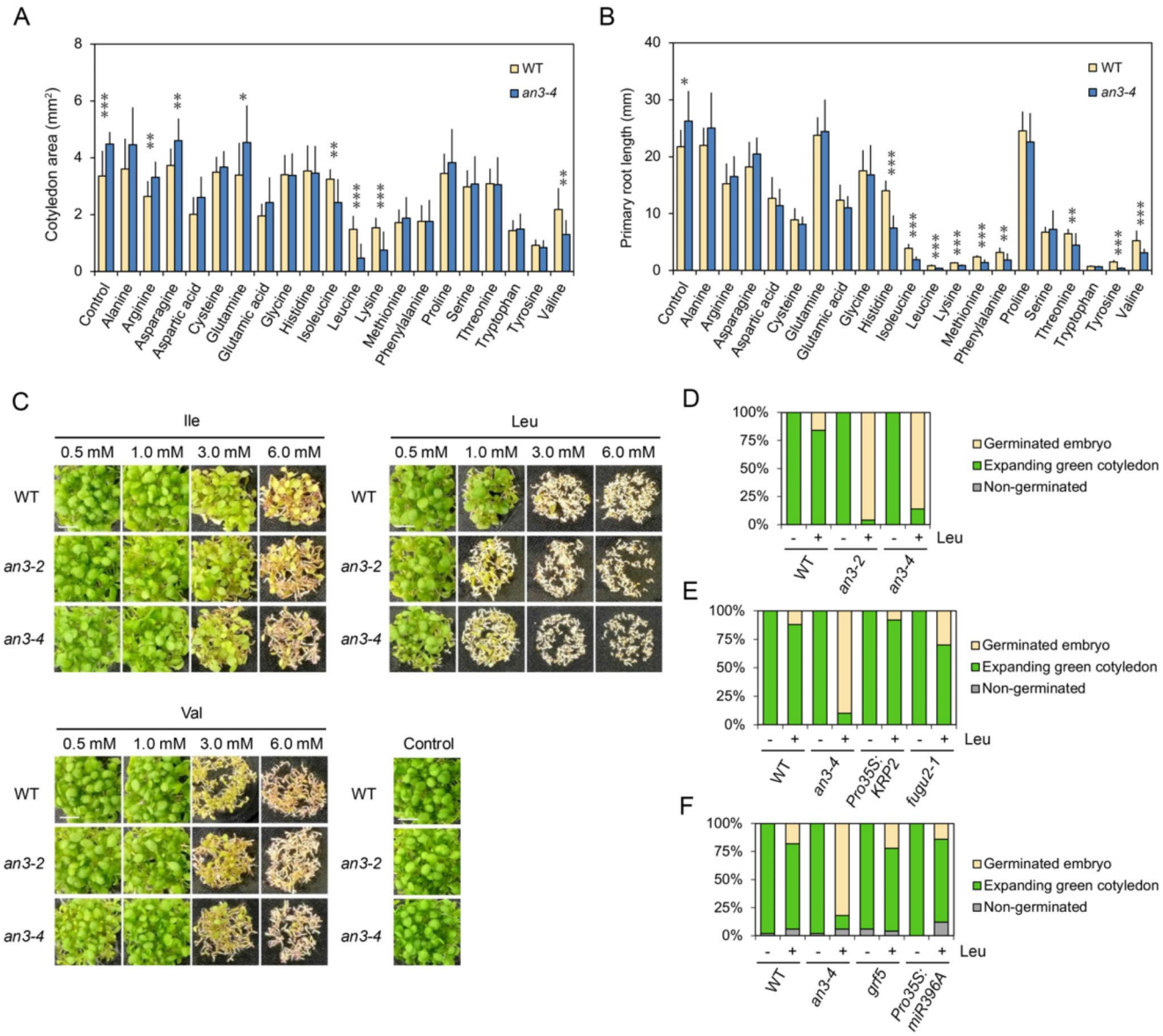

Fig. 1 Suppression of seedling growth by amino acids in *an3* mutants. **A** and **B** Effects of exogenous amino acids on cotyledon area and primary root length. Wild-type (WT) and *an3-4* seedlings were grown on half-strength Murashige and Skoog (MS) medium containing 1.0 mM of each amino acid for 6 days. Data are means ± standard deviation (s.d.) ($n = 12$). Asterisks indicate significant differences between WT and *an3-4* seedlings (*$P < 0.05$; **$P < 0.01$; ***$P < 0.001$; Student's t-test). **C** Concentration dependency of Ile, Leu, and Val on seedling growth suppression. WT, *an3-2*, and *an3-4* seedlings were grown on half-strength MS medium containing 0 (control), 0.5, 1.0, 3.0, or 6.0 mM of each branched-chain amino acid (BCAA) for 7 days. Scale bars = 1.0 cm. **D–F** Effects of exogenous Leu treatment on seedling establishment. WT, *an3-2*, and *an3-4* mutants (**D**); WT, *an3-4*, *Pro35S:KRP2*, and *fugu2-1* mutants (**E**); and WT, *an3-4*, *grf5*, and *Pro35S:MIR396A* seedlings (**F**) were grown on half-strength MS medium containing 1.0 mM Leu for 7 days. Data are proportions for each growth category ($n = 50$)

which is a direct degradation product of Leu, were lower in *an3* seedlings than in WT seedlings, particularly under Leu treatment (Fig. 2B). In contrast, the levels of 3-methylbutanoyl-CoA, which is derived from 4-methyl-2-oxovaleric acid, were comparable between WT and *an3* seedlings, regardless of Leu treatment (Fig. 2B). These findings suggest that the Leu degradation pathway is impacted, at least at the initial degradation step, in Leu-treated *an3* mutants.

To further assess the relationship between the transcript and metabolite profiles with physiological implications, we performed correlation analysis of our transcriptome data with publicly available data using the *Arabidopsis thaliana* transcriptome profile correlation analysis tool (AtCAST) (Kakei & Shimada, 2015). The result suggested that the global transcriptional profiles of the *an3* mutants were associated with hypoxia response signatures (Supplemental

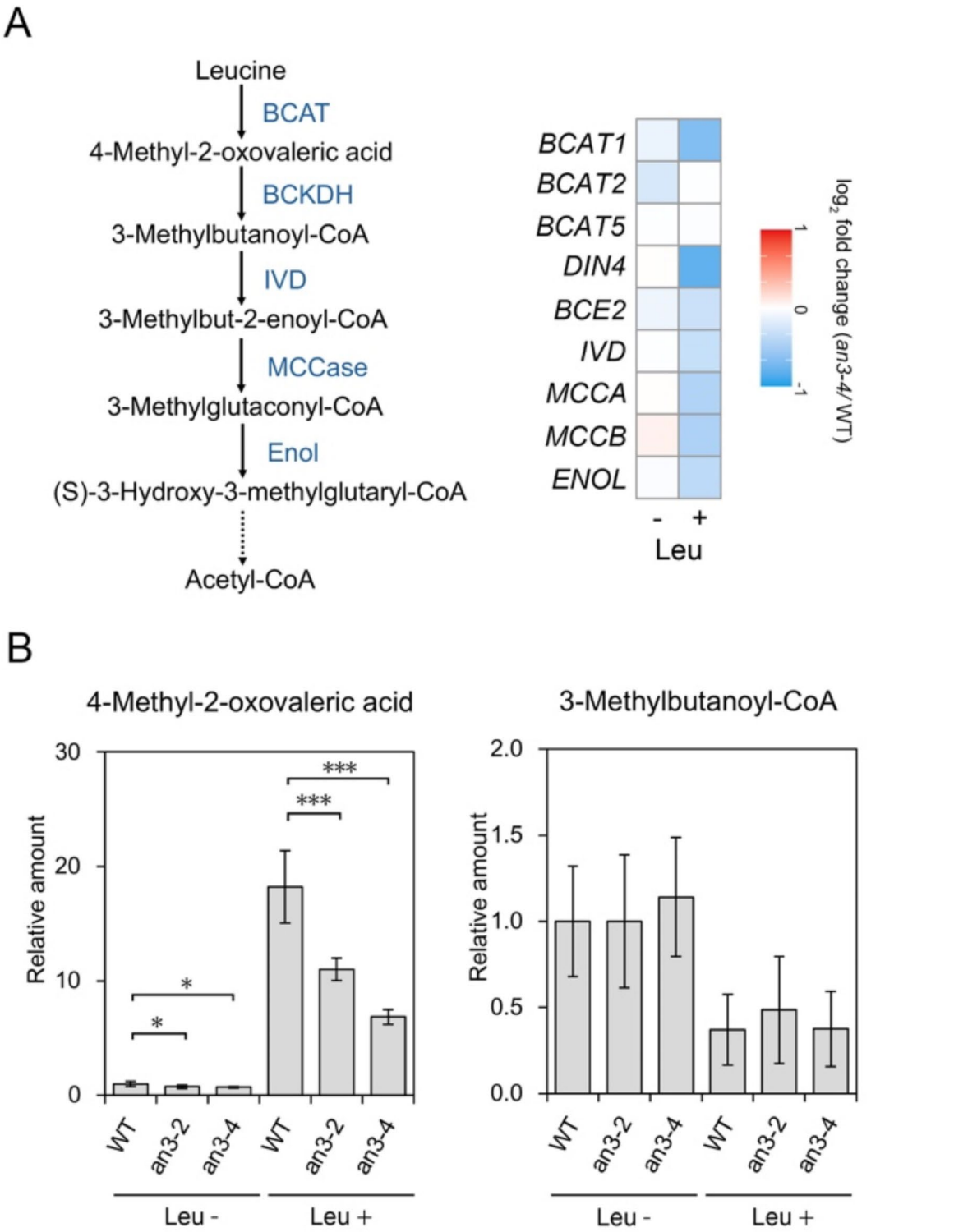

Fig. 2 Effects of *an3* mutation on the leucine degradation pathway. **A** Schematic diagram of the Leu degradation pathway. Related enzymes in Arabidopsis are indicated in blue (left). BCAT, branched-chain amino acid transferase; BCKDH, branched-chain ketoacid dehydrogenase; IVD, isovaleryl-coenzyme A (CoA) dehydrogenase; MCCase, 3-methylcrotonyl-CoA carboxylase; Enol, enoyl-CoA hydratase. Heatmap shows transcript levels of putative Leu catabolic genes (right). *DARK INDUCIBLE 4* (*DIN4*) and *BCKDH E2* (*BCE2*) encode the BCKDH E1b and E2 subunits, respectively (Fujiki et al., 2000). **B** Relative amounts of 4-methyl-2-oxovaleric acid and 3-methylbutanoyl-CoA in WT, *an3-2*, and *an3-4* seedlings analyzed using the LC-MS/MS system. Data are means ± s.d. ($n = 3$). Asterisks indicate significant differences (*$P < 0.05$; **$P < 0.01$; ***$P < 0.001$; Student's t-test)

Table. S3). GO enrichment analysis showed significant enrichment in cellular response to hypoxia and hydrogen peroxide catabolic processes among genes upregulated in the *an3* mutants, regardless of Leu treatment (Fig. 3A, B). These upregulated genes included the hypoxia-related genes *PYRUVATE DECARBOXYLASE 1* (*PDC1*) and *ALCOHOL DEHYDROGENASE 1* (*ADH1*) (Gibbs et al., 2011) (Supplemental Table. S4). There was also significant enrichment in GO categories for photosynthetic and light response processes among genes downregulated in the *an3* mutants under Leu treatment (Fig. 3C), with no significant changes observed under untreated conditions.

We conducted a GC-MS-based metabolome analysis to determine whether transcriptional changes related to the hypoxia response affect *an3* mutant metabolism (Supplemental Table. S5). Principal component analysis of the 88 detected metabolites across the samples indicated a clear difference in global metabolite profiles between the treated and untreated conditions (Fig. 4A). We also observed a trend suggesting distinct metabolite profiles between the WT and *an3* mutant seedlings in the Leu-treated condition (Fig. 4A). Our analysis showed that the abundance of nine metabolites significantly increased in both Leu-treated and untreated *an3-4* seedlings compared to WT (Fig. 4B and C), including L-phenylalanine (Phe), L-alanine (Ala), and γ-aminobutyric acid (GABA) (Fig. 4D–F), which are known to accumulate in response to hypoxia (Lothier et al., 2020; Miyashita & Good, 2008). Conversely, no metabolites decreased in both the treated and untreated *an3* mutant seedlings compared to WT (Fig. 4B and C). These results, alongside the detected changes in the Leu degradation pathway, support the hypothesis that the *an3* seedlings exhibit a hypoxia-like response.

3.3 Altered ROS distribution in *an3* root tips

Hypoxia response interacts with the regulation of cellular ROS levels (Bailey-Serres et al., 2012; Gibbs et al., 2015). ROS distribution plays an important role in regulating root growth, with superoxide (O_2^-) and hydrogen peroxide (H_2O_2) predominantly accumulating in the meristematic and differentiation zones, respectively (Tsukagoshi et al., 2010; Yamada et al., 2020). To determine whether ROS distribution is compromised in *an3* seedlings, which exhibit a hypoxia-like response even under untreated conditions, we performed NBT staining to compare the distribution of superoxide (O_2^-) between WT and *an3* mutant seedlings. We observed that NBT staining more expanded in the root

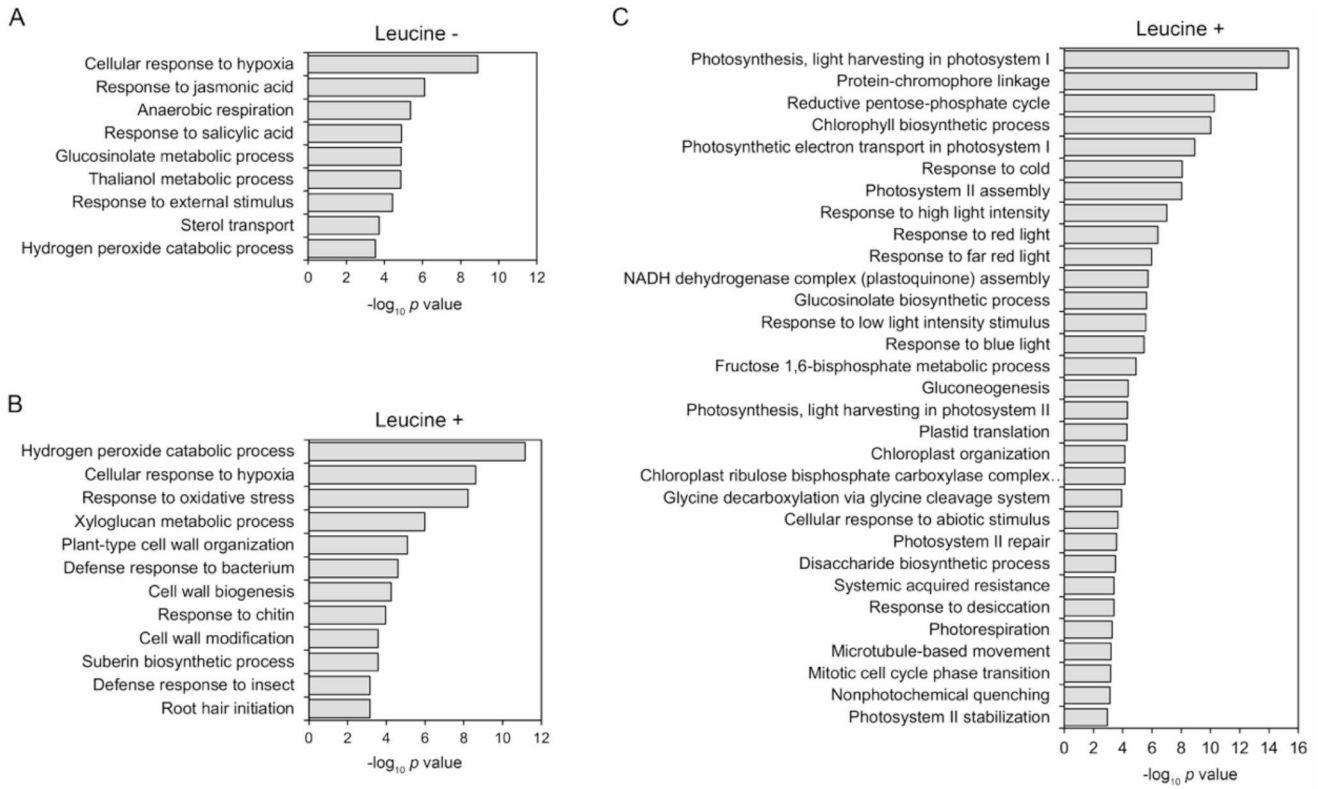

Fig. 3 Gene Ontology (GO) enrichment analysis of transcriptome data. **A**–**C** Significantly enriched PANTHER GO-slim biological process terms for upregulated differentially expressed genes (DEGs) extracted from seedlings cultured under Leu-untreated (**A**) and 1.0 mM Leu-treated conditions (**B**), and downregulated DEGs extracted from seedlings cultured under the 1.0 mM Leu-treated condition (**C**). No GO category was significantly enriched in the downregulated DEGs extracted from seedlings cultured under the Leu-untreated conditions

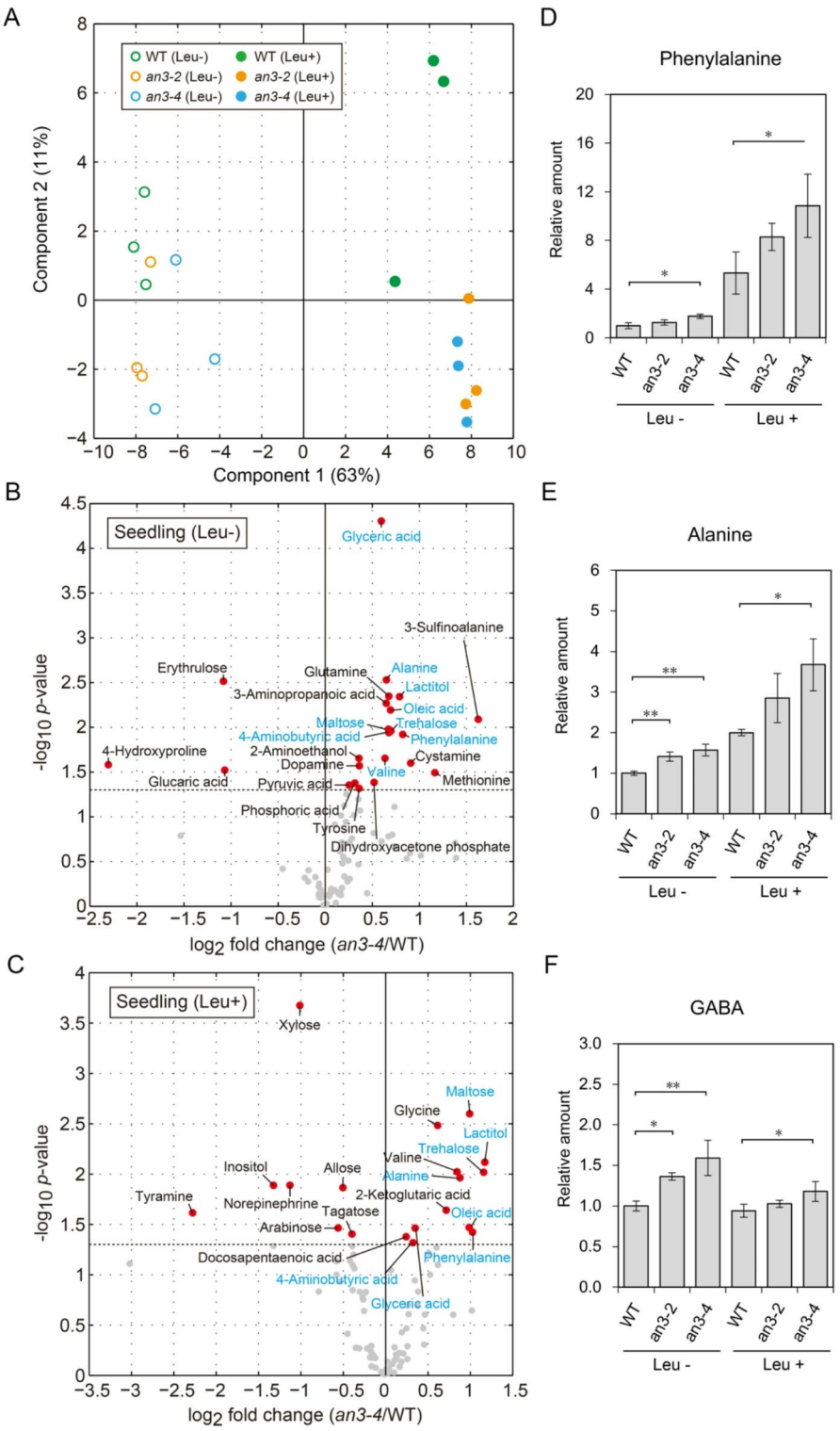

Fig. 4 Metabolite profiling of WT and *an3* seedlings cultured under Leu-treated and untreated conditions. **A** Principal component analysis of 88 metabolites detected across all tested samples by GC-MS-based metabolome analysis. Circles represent individual samples from WT, *an3-2*, and *an3-4* seedlings ($n=3$). **B** and **C** Volcano plots of metabolic changes between the WT and *an3-4* seedlings under Leu-untreated (**B**) and Leu-treated conditions (**C**). Dots represent means of three biological replicates. Red dots indicate significantly increased or decreased metabolites in *an3-4* mutants ($P<0.05$; Welch's t-test). Significantly increased metabolites under both Leu-untreated and Leu-treated conditions are highlighted in blue. **D–F** Relative amounts of phenylalanine (**D**), alanine (**E**), and GABA (**F**) in WT, *an3-2*, and *an3-4* seedlings. Data were obtained through GC-MS-based metabolome analysis. Data are means ± s.d. ($n=3$). Asterisks indicate significant differences (*$P<0.05$; **$P<0.01$; Student's t-test)

tips of *an3* mutants than in those of WT plants (Fig. 5A). Correspondingly, BES-H_2O_2-Ac fluorescence, which indicates the distribution of hydrogen peroxide (H_2O_2), shifted shootward in the root tips of *an3* mutants (Fig. 5B). Additionally, NO levels examined with DAF-2 DA fluorescence were found to decrease in the root tips of *an3* seedlings (Fig. 5C), further indicating that ROS distribution is altered in the *an3* seedlings.

Given the altered distribution of ROS in root tips and the growth suppression observed in the *an3-4* mutants, we investigated whether *AN3* is expressed in the root tips in our experimental context as previously reported (Ercoli

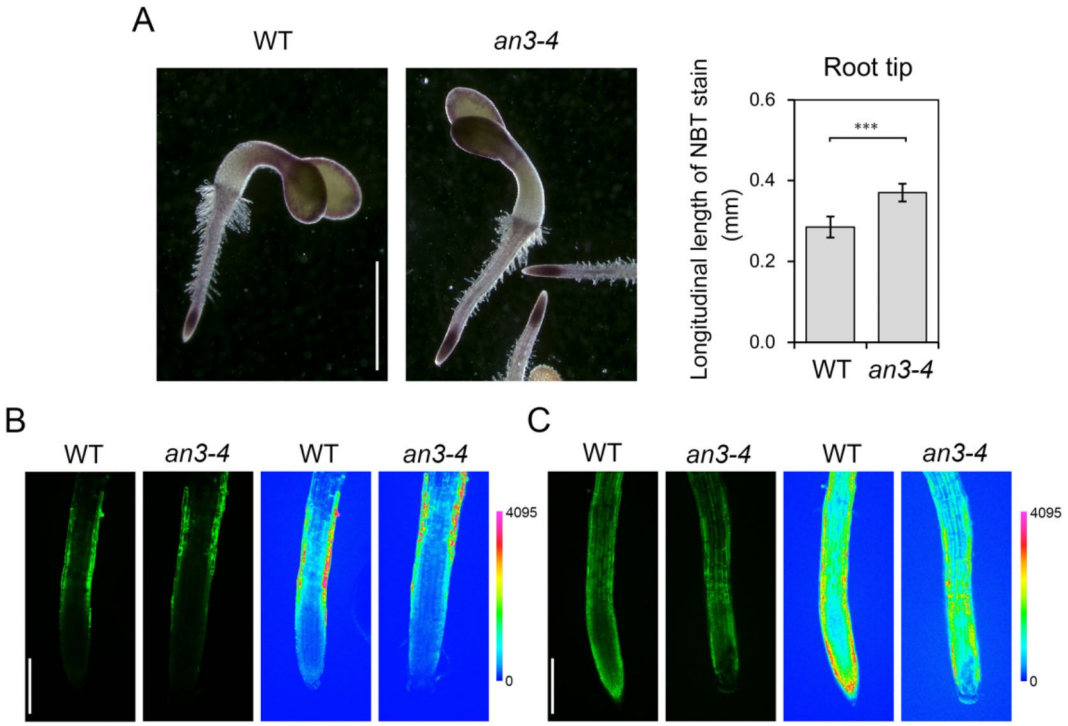

Fig. 5 Imaging-based reactive oxygen species (ROS) detection in WT and *an3-4* roots. **A** Nitroblue tetrazolium (NBT)-stained images of WT and *an3-4* seedlings (left). Length of NBT-stained regions along the root developmental axis is shown (right). Data are means ± s.d. ($n = 5$). Asterisk indicates significant difference (***$P < 0.001$; Student's t-test). **B** and **C** BES-H_2O_2-Ac fluorescence (**B**) and diaminofluorescein-2 diacetate (DAF-2 DA)-fluorescence (**C**) images of WT and *an3-4* root tips. Heatmaps indicate fluorescence intensity levels in the corresponding images. Scale bars = 1.0 mm (**A**) and 200 µm (**B** and **C**)

et al., 2018). We examined the *an3-4/ProAN3:AN3-GFP* transgenic lines, in which *AN3-GFP* is expressed under the *AN3* promoter in the *an3-4* genetic background (Kawade et al., 2013). This genomic fragment functioned as a promoter of the *AN3* gene during seedling growth in our experimental context, as demonstrated by the alleviation of growth suppression by Leu in the *an3-4/ProAN3:AN3-GFP* transgenic lines compared to *an3-4* mutants (Fig. 6A). We confirmed the presence of AN3-GFP fluorescence in root tips of the *an3-4/ProAN3:AN3-GFP* transgenic line (Fig. 6B). A similar expression pattern was observed in the β-glucuronidase (GUS)-reporter lines, *ProAN3:GUS* and *an3-4/ProAN3:GUS* (Kawade et al., 2013), in which GUS staining was primarily detected in the root tips of seedlings (Fig. 6C). These observations indicate that the *AN3* gene is predominantly expressed in root tips during the seedling growth.

4 Discussion

In this study, we found that *an3* mutants are more susceptible to Leu-induced suppression of seedling growth compared to WT plants. Our multi-omics analysis identified molecular signatures suggesting a hypoxia-like response in *an3* mutants. Consistently, ROS distribution was altered in the root tips of *an3* mutants. These results suggest that *AN3* might be linked to promote seedling growth through metabolic and/or physiological modulations in Arabidopsis.

We previously demonstrated that *Ppan3* mutants of *Physcomitrium patens* exhibited stunted shoot growth and excessive accumulation of Arg. This growth suppression was also observed in WT shoots when cultured with Arg (Kawade et al., 2020). Given the interaction of *PpAN3* signaling with amino acid metabolism, we explored amino acids relevant to *AN3*-mediated tissue growth in Arabidopsis. Our screening revealed that BCAAs and Lys, but not Arg, significantly compromised seedling growth, particularly in the *an3* genetic background. Although the specific amino acids involved differ between *Physcomitrium patens* and Arabidopsis and this discrepancy is hard to explain based on our current knowledge, these findings suggest a possible link in which *AN3* signaling contributes to tissue growth via metabolic and/or physiological modulation. As the Leu degradation pathway was disturbed at both the transcriptional and metabolic levels in *an3* seedlings, this metabolic disorder may be linked to the suppression of seedling growth by Leu. Future research is needed to elucidate the mechanism by which *AN3* signaling contributes to transcriptional and metabolic regulation during seedling growth by identifying its

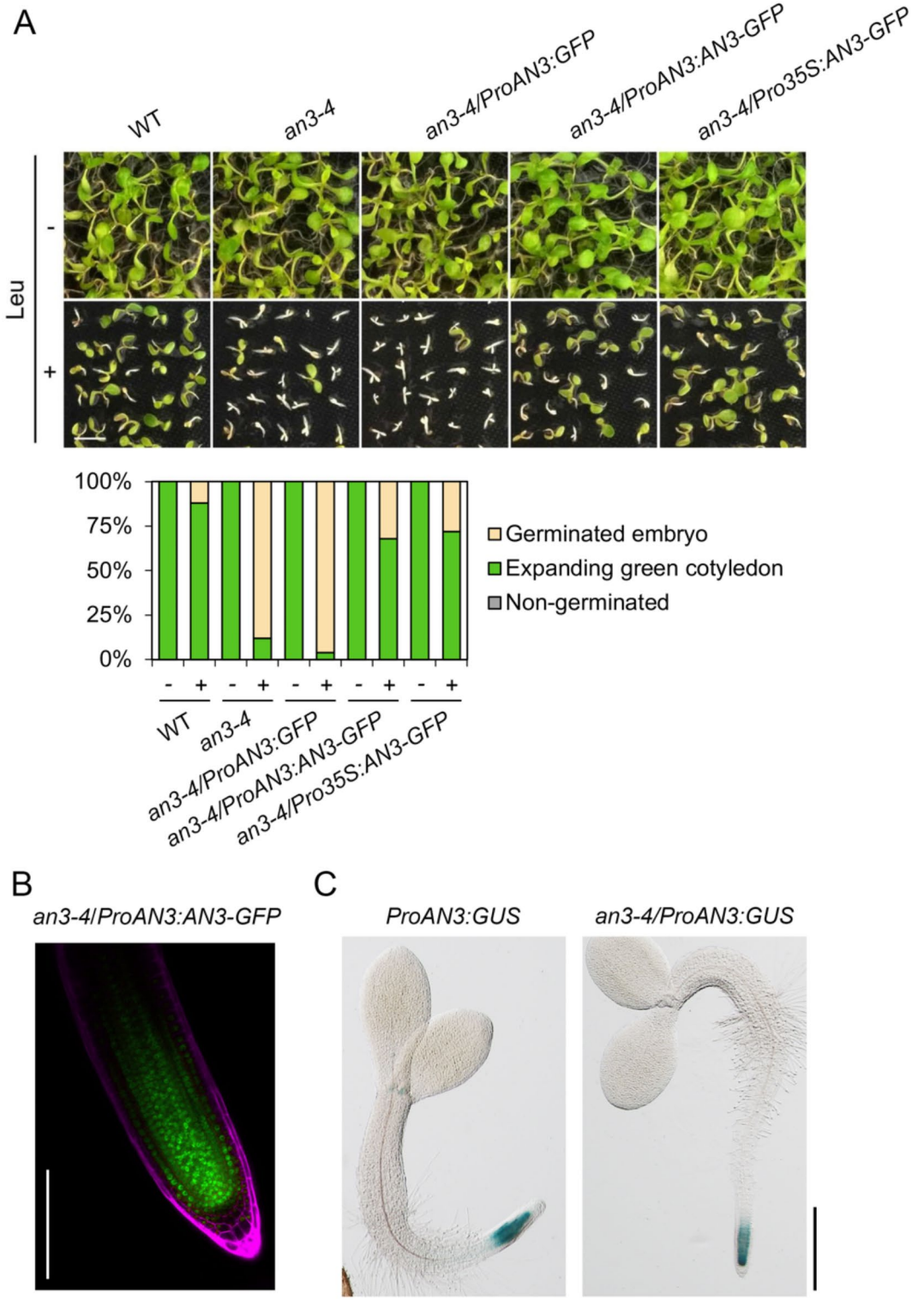

Fig. 6 Expression of *AN3* in root tips. **A** Effects of exogenous Leu treatment on seedling establishment. WT, *an3-4*, *an3-4/ProAN3:GFP*, *an3-4/ProAN3:AN3-GFP*, and *an3-4/Pro35S:AN3-GFP* were grown on half-strength MS medium containing 1.0 mM Leu for 7 days. Data are proportions of each growth category ($n = 50$). **B** AN3-GFP fluorescence (green) and propidium iodide staining (magenta) in root tips of *an3-4/ProAN3:AN3-GFP* transgenic line. **C** β-glucuronidase (GUS) expression patterns in seedlings of *ProAN3:GUS* and *an3-4/ProAN3:GUS* transgenic lines. Scale bars = 1.0 cm (**A**), 100 μm (**B**), and 500 μm (**C**)

downstream signaling components. The experiments would include multi-omics analysis with higher resolution in time (time-series sampling) and space (cell and/or tissue isolation) because we analyzed the whole seedlings at only the growth-arrested stage in this study. Such an analysis would help to determine whether the Leu treatment in this study disturbed the regulatory mechanisms of seedling growth or merely arrested basal cellular activity that might become more susceptible under the *an3* genetic background.

In addition to metabolic disorder in the Leu degradation pathway, we found that *an3* mutants exhibited a hypoxia-like response, as suggested by the upregulation of genes involved in the cellular response to hypoxia and the accumulation of relevant amino acids including Phe, Ala, and GABA (Lothier et al., 2020; Miyashita & Good, 2008). Our experiments detected altered ROS distribution, further supporting the notion that cellular oxygen conditions are disturbed in *an3* mutants. Although the mechanistic and functional interactions between Leu hypersensitivity and the hypoxia response remain elusive, one potential link could be the involvement of the N-end rule pathway of proteolysis in seedling growth. This targeted proteolysis is crucial for sensing oxygen levels, which in turn regulates the cellular response to hypoxia (Gibbs et al., 2011). The hypoxia response then modulates respiration, the tricarboxylic acid (TCA) cycle, and amino acid metabolism through the stabilization of the RAP2.12 protein (Paul et al., 2016). Additionally, since BCAA degradation in mitochondria provides an alternative substrate for mitochondrial respiration under stressed conditions (Araújo et al., 2011; Hildebrandt et al., 2015; Ishizaki et al., 2005; Schertl et al., 2017), *an3* mutants may experience an energy shortage for seedling growth due to impaired Leu degradation when subjected to hypoxia. It would be interesting to investigate whether seedling growth is adjusted in response to oxygen levels and the mechanism by which Leu metabolism is linked to this process. Functional and phenotypic analyses of the mutants constitutively exhibiting hypoxia response and their double mutants with *an3* are awaited to address this idea because this study showed the growth, transcriptome, and metabolome profiles only from the *an3* single mutants.

AN3 was originally identified as a transcriptional co-activator for cell proliferation in leaves (Horiguchi et al., 2005; Kim & Kende, 2004). Although less attention has been paid to the role of *AN3* in root development, recent studies have shown that *AN3* regulates cell proliferation in the root apical meristem (Ercoli et al., 2018; Xiong et al., 2020). We also confirmed *AN3* expression in the root tips. Given that cell proliferation is regulated by ROS distribution in the root apical meristem (Tsukagoshi et al., 2010; Yamada et al., 2020), the impaired control of ROS distribution may be relevant for the growth defect observed in the *an3* roots. As no previous study has reported molecular signatures related to ROS distribution in the transcriptome of *an3* leaves (Ezaki et al., 2024; Horiguchi et al., 2011; Kawade et al., 2020; Nelissen et al., 2015; Vercruyssen et al., 2014), the phenotypes observed in this study may be tissue context-dependent. These findings prompt a detailed investigation into the role of *AN3* in roots, from the perspective of the control of oxidative status. Because *AN3* is expressed in the root tips, future experiments should confirm whether our observation becomes more obvious when using the root tips as tissue samples for transcriptome and metabolome analyses.

Supplementary Information The online version contains supplementary material available at https://doi.org/10.1007/s11306-025-02249-9.

Acknowledgements We thank C. Yamaguchi (ExCELLS) for help with the experiments; Model Plant Section, Model Organisms Facility (Trans-Scale Biology Center, NIBB) for technical support; Optics and Imaging Facility, (Trans-Scale Biology Center, NIBB) for the access to confocal microscope; M. Matsumoto (NIBB) in Trans-Omics Facility (Trans-Scale Biology Center, NIBB) for RNA-sequencing; NIBB Collaborative Research Program (16NIBB444). This work was supported by BIO-NEXT project from Exploratory Research Center on Life and Living Systems (ExCELLS); Japan Society for the Promotion of Science (JSPS) KAKENHI Grant Numbers JP17K15147 and JP22K06289.

Author contributions KK and MN conceived and designed the research. KK, MN, TM, KY, MO, HT, and SS conducted experiments. GH contributed new plant materials. KK and MN analyzed data. KK wrote the manuscript with inputs from all other authors. All authors read and approved the manuscript.

Funding Open Access funding provided by Saitama University.

Data availability Raw sequencing data are available via the DNA Data Bank of Japan (DDBJ) BioProject (PRJDB18188).

Declarations

Conflict of interest The authors declare no competing interests.

Ethical approval This article does not contain any studies with human and/or animal participants performed by any of the authors.

References

Angelovici, R., Lipka, A. E., Deason, N., Gonzalez-Jorge, S., Lin, H., Cepela, J., et al. (2013). Genome-wide analysis of branched-chain amino acid levels in *Arabidopsis* seeds. *The Plant Cell*, *25*, 4827–4843. https://doi.org/10.1105/tpc.113.119370

Araújo, W. L., Tohge, T., Ishizaki, K., Leaver, C. J., & Fernie, A. R. (2011). Protein degradation - an alternative respiratory substrate for stressed plants. *Trends in Plant Science*, *16*, 489–498. https://doi.org/10.1016/j.tplants.2011.05.008

Bailey-Serres, J., Fukao, T., Gibbs, D. J., Holdsworth, M. J., Lee, S. C., Licausi, F., et al. (2012). Making sense of low oxygen sensing. *Trends in Plant Science*, *17*, 129–138. https://doi.org/10.1016/j.tplants.2011.12.004

De Veylder, L., Beeckman, T., Beemster, G. T., Krols, L., Terras, F., Landrieu, I., et al. (2001). Functional analysis of cyclin-dependent kinase inhibitors of Arabidopsis. *The Plant Cell*, *13*, 1653–1668. https://doi.org/10.1105/tpc.010087

Donnelly, P. M., Bonetta, D., Tsukaya, H., Dengler, R. E., & Dengler, N. G. (1999). Cell cycling and cell enlargement in developing leaves of *Arabidopsis*. *Developmental Biology*, *215*, 407–419. https://doi.org/10.1006/dbio.1999.9443

Dunand, C., Crèvecoeur, M., & Penel, C. (2007). Distribution of superoxide and hydrogen peroxide in *Arabidopsis* root and their influence on root development: Possible interaction with peroxidases. *New Phytologist*, *174*, 332–341. https://doi.org/10.1111/j.1469-8137.2007.01995.x

Ercoli, M. F., Ferela, A., Debernardi, J. M., Perrone, A. P., Rodriguez, R. E., & Palatnik, J. F. (2018). GIF transcriptional coregulators control root meristem homeostasis. *The Plant Cell*, *30*, 347–359. https://doi.org/10.1105/tpc.17.00856

Ezaki, K., Koga, H., Takeda-Kamiya, N., Toyooka, K., Higaki, T., Sakamoto, S., et al. (2024). Precocious cell differentiation occurs in proliferating cells in leaf primordia in Arabidopsis *angustifolia3* mutant. *Frontiers in Plant Science*, *15*, 1322223. https://doi.org/10.3389/fpls.2024.1322223

Ferjani, A., Horiguchi, G., Yano, S., & Tsukaya, H. (2007). Analysis of leaf development in *Fugu* mutants of Arabidopsis reveals three compensation modes that modulate cell expansion in determinate organs. *Plant Physiology*, *144*, 988–999. https://doi.org/10.1104/pp.107.099325

Fujiki, Y., Sato, T., Ito, M., & Watanabe, A. (2000). Isolation and characterization of cDNA clones for the E1b and E2 subunits of the branched-chain alpha-ketoacid dehydrogenase complex in *Arabidopsis*. *Journal of Biological Chemistry*, *275*, 6007–6013. https://doi.org/10.1074/jbc.275.8.6007

Gibbs, D. J., Conde, J. V., Berckhan, S., Prasad, G., Mendiondo, G. M., & Holdsworth, M. J. (2015). Group VII ethylene response factors coordinate oxygen and nitric oxide signal transduction and stress responses in plants. *Plant Physiology*, *169*, 23–31. https://doi.org/10.1104/pp.15.00338

Gibbs, D. J., Lee, S. C., Md Isa, N., Gramuglia, S., Fukao, T., Bassel, G. W., et al. (2011). Homeostatic response to hypoxia is regulated by the N-end rule pathway in plants. *Nature*, *479*, 415–418. https://doi.org/10.1038/nature10534

Hildebrandt, T. M., Nunes Nesi, A., Araújo, W. L., & Braun, H. P. (2015). Amino acid catabolism in plants. *Molecular Plant*, *8*, 1563–1579. https://doi.org/10.1016/j.molp.2015.09.005

Hisanaga, T., Ferjani, A., Horiguchi, G., Ishikawa, N., Fujikura, U., Kubo, M., et al. (2013). The ATM-dependent DNA damage response acts as an upstream trigger for compensation in the *fas1* mutation during Arabidopsis leaf development. *Plant Physiology*, *162*, 831–841. https://doi.org/10.1104/pp.113.216796

Horiguchi, G., Kim, G. T., & Tsukaya, H. (2005). The transcription factor AtGRF5 and the transcription coactivator AN3 regulate cell proliferation in leaf primordia of *Arabidopsis Thaliana*. *The Plant Journal*, *43*, 68–78. https://doi.org/10.1111/j.1365-313X.2005.02429.x

Horiguchi, G., Nakayama, H., Ishikawa, N., Kubo, M., Demura, T., Fukuda, H., et al. (2011). *ANGUSTIFOLIA3* plays roles in adaxial/abaxial patterning and growth in leaf morphogenesis. *Plant & Cell Physiology*, *52*, 112–124. https://doi.org/10.1093/pcp/pcq178

Hussain, E., Romanowski, A., & Halliday, K. J. (2022). PIF7 controls leaf cell proliferation through an AN3 substitution repression mechanism. *Proceedings of National Academy of Sciences USA*, *119*(e2115682119). https://doi.org/10.1073/pnas.2115682119

Ishizaki, K., Larson, T. R., Schauer, N., Fernie, A. R., Graham, I. A., & Leaver, C. J. (2005). The critical role of *Arabidopsis* electron-transfer Flavoprotein: Ubiquinone oxidoreductase during dark-induced starvation. *The Plant Cell*, *17*, 2587–2600. https://doi.org/10.1105/tpc.105.035162

Kakei, Y., & Shimada, Y. (2015). AtCAST3.0 update: A web-based tool for analysis of transcriptome data by searching similarities in gene expression profiles. *Plant & Cell Physiology*, *56*, e7. https://doi.org/10.1093/pcp/pcu174

Kawade, K., Horiguchi, G., Hirose, Y., Oikawa, A., Hirai, M. Y., Saito, K., et al. (2020). Metabolic control of gametophore shoot formation through arginine in the moss *Physcomitrium patens*. *Cell Reports*, *32*, 108127. https://doi.org/10.1016/j.celrep.2020.108127

Kawade, K., Horiguchi, G., Usami, T., Hirai, M. Y., & Tsukaya, H. (2013). ANGUSTIFOLIA3 signaling coordinates proliferation between clonally distinct cells in leaves. *Current Biology*, *23*, 788–792. https://doi.org/10.1016/j.cub.2013.03.044

Kawade, K., Li, Y., Koga, H., Sawada, Y., Okamoto, M., Kuwahara, A., Tsukaya, H., & Hirai, M. Y. (2018). The cytochrome P450 CYP77A4 is involved in auxin-mediated patterning of the *Arabidopsis Thaliana* embryo. *Development*, *145*, dev168369. https://doi.org/10.1242/dev.168369

Kawade, K., Tabeta, H., Ferjani, A., & Hirai, M. Y. (2023). The roles of functional amino acids in plant growth and development. *Plant & Cell Physiology*, *64*, 1482–1493. https://doi.org/10.1093/pcp/pcad071

Kim, D., Pertea, G., Trapnell, C., Pimentel, H., Kelley, R., & Salzberg, S. L. (2013). TopHat2: Accurate alignment of transcriptomes in the presence of insertions, deletions and gene fusions. *Genome Biology*, *14*, R36. https://doi.org/10.1186/gb-2013-14-4-r36

Kim, J. H., & Kende, H. (2004). A transcriptional coactivator, AtGIF1, is involved in regulating leaf growth and morphology in Arabidopsis. *Proceedings of National Academy of Sciences USA*, *101*, 13374–13379. https://doi.org/10.1073/pnas.0405450101

Kojima, H., Nakatsubo, N., Kikuchi, K., Kawahara, S., Kirino, Y., Nagoshi, H., et al. (1998). Detection and imaging of nitric oxide with novel fluorescent indicators: Diaminofluoresceins. *Analytical Chemistry*, *70*, 2446–2453. https://doi.org/10.1021/ac9801723

Lothier, J., Diab, H., Cukier, C., Limami, A. M., & Tcherkez, G. (2020). Metabolic responses to waterlogging differ between roots and shoots and reflect phloem transport alteration in *Medicago truncatula*. *Plants*, *9*, 1373. https://doi.org/10.3390/plants9101373

Martin, M. (2011). Cutadapt removes adapter sequences from high-throughput sequencing reads. *EMBnet Journal*, *17*, 10–12. https://doi.org/10.14806/ej.17.1.200

Mi, H., Muruganujan, A., Ebert, D., Huang, X., & Thomas, P. D. (2019). PANTHER version 14: More genomes, a new PANTHER GO-slim and improvements in enrichment analysis tools. *Nucleic Acids Research*, *47*, D419–D426. https://doi.org/10.1093/nar/gky1038

Miyashita, Y., & Good, A. G. (2008). Contribution of the GABA shunt to hypoxia-induced Alanine accumulation in roots of *Arabidopsis Thaliana*. *Plant & Cell Physiology*, *49*, 92–102. https://doi.org/10.1093/pcp/pcm171

Murashige, T., & Skoog, F. (1962). A revised medium for rapid growth and bio assays with tobacco tissue cultures. *Physiologia Plantarum*, *15*, 473–497. https://doi.org/10.1111/j.1399-3054.1962.tb08052.x

Nelissen, H., Eeckhout, D., Demuynck, K., Persiau, G., Walton, A., van Bel, M., et al. (2015). Dynamic changes in ANGUSTIFOLIA3 complex composition reveal a growth regulatory mechanism in the maize leaf. *The Plant Cell*, *27*, 1605–1619. https://doi.org/10.1105/tpc.15.00269

Okamura, M., Hirai, M. Y., Sawada, Y., Okamoto, M., Oikawa, A., Sasaki, R., Arai-Sanoh, Y., Mukouyama, T., Adachi, S., & Kondo, M. (2021). Analysis of carbon flow at the metabolite level reveals that starch synthesis from hexose is a limiting factor in a high-yielding rice cultivar. *Journal of Experimental Botany*, *72*, 2570–2583. https://doi.org/10.1093/jxb/erab016

Paul, M. V., Iyer, S., Amerhauser, C., Lehmann, M., van Dongen, J. T., & Geigenberger, P. (2016). Oxygen sensing via the ethylene response transcription factor RAP2.12 affects plant metabolism and performance under both normoxia and hypoxia. *Plant Physiology*, *172*, 141–153. https://doi.org/10.1104/pp.16.00460

Rodriguez, R. E., Mecchia, M. A., Debernardi, J. M., Schommer, C., Weigel, D., & Palatnik, J. F. (2010). Control of cell proliferation in *Arabidopsis Thaliana* by MicroRNA miR396. *Development*, *137*, 103–112. https://doi.org/10.1242/dev.043067

Schertl, P., Danne, L., & Braun, H. P. (2017). 3-Hydroxyisobutyrate dehydrogenase is involved in both, valine and isoleucine degradation in *Arabidopsis Thaliana*. *Plant Physiology*, *175*, 51–61. https://doi.org/10.1104/pp.17.00649

Tabeta, H., Higashi, Y., Okazaki, Y., Toyooka, K., Wakazaki, M., Sato, M., et al. (2022). Skotomorphogenesis exploits threonine to promote hypocotyl elongation. *Quantitative Plant Biology*, *3*, e26. https://doi.org/10.1017/qpb.2022.19

Tomoi, T., Kawade, K., Kitagawa, M., Sakata, Y., Tsukaya, H., & Fujita, T. (2020). Quantitative imaging reveals distinct contributions of SnRK2 and ABI3 in plasmodesmata permeability in *Physcomitrella patens*. *Plant & Cell Physiology*, *61*(5), 942–956. https://doi.org/10.1093/pcp/pcaa021

Toyokura, K., Watanabe, K., Oiwaka, A., Kusano, M., Tameshige, T., Tatematsu, K., et al. (2011). Succinic semialdehyde dehydrogenase is involved in the robust patterning of Arabidopsis leaves along the adaxial–abaxial axis. *Plant & Cell Physiology*, *52*, 1340–1353. https://doi.org/10.1093/pcp/pcr079

Trapnell, C., Williams, B. A., Pertea, G., Mortazavi, A., Kwan, G., van Baren, M. J., et al. (2010). Transcript assembly and quantification by RNA-Seq reveals unannotated transcripts and isoform switching during cell differentiation. *Nature Biotechnology*, *28*, 511–515. https://doi.org/10.1038/nbt.1621

Tsugawa, H., Kanazawa, M., Ogiwara, A., & Arita, M. (2014). MRMPROBS suite for metabolomics using large-scale MRM assays. *Bioinformatics*, *30*, 2379–2380. https://doi.org/10.1093/bioinformatics/btu203

Tsukagoshi, H., Busch, W., & Benfey, P. N. (2010). Transcriptional regulation of ROS controls transition from proliferation to differentiation in the root. *Cell*, *143*, 606–616. https://doi.org/10.1016/j.cell.2010.10.020

Vercruyssen, L., Verkest, A., Gonzalez, N., Heyndrickx, K. S., Eeckhout, D., Han, S. K., et al. (2014). ANGUSTIFOLIA3 binds to SWI/SNF chromatin remodeling complexes to regulate transcription during *Arabidopsis* leaf development. *The Plant Cell*, *26*, 210–229. https://doi.org/10.1105/tpc.113.115907

Verkest, A., Manes, C. L., de Vercruysse, O., Maes, S., Van Der Schueren, S., Beeckman, E., T., et al. (2005). The cyclin-dependent kinase inhibitor KRP2 controls the onset of the endoreduplication cycle during Arabidopsis leaf development through Inhibition of mitotic CDKA;1 kinase complexes. *The Plant Cell*, *17*, 1723–1736. https://doi.org/10.1105/tpc.105.032383

Wang, M., Tabeta, H., Ohtaka, K., Kuwahara, A., Nishihama, R., Ishikawa, T., et al. (2024). The phosphorylated pathway of Serine biosynthesis affects sperm, embryo, and sporophyte development, and metabolism in *Marchantia polymorpha*. *Communications Biology*, *7*, 102. https://doi.org/10.1038/s42003-023-05746-6

Xiong, F., Zhang, B. K., Liu, H. H., Wei, G., Wu, J. H., Wu, Y. N., et al. (2020). Transcriptional regulation of *PLETHORA1* in the root meristem through an importin and its two antagonistic cargos. *The Plant Cell*, *32*, 3812–3824. https://doi.org/10.1105/tpc.20.00108

Yamada, M., Han, X., & Benfey, P. N. (2020). RGF1 controls root meristem size through ROS signalling. *Nature*, *577*, 85–88. https://doi.org/10.1038/s41586-019-1819-6

Zheng, L., Wu, H., Wang, A., Zhang, Y., Liu, Z., Ling, H. Q., et al. (2023). The SOD7/DPA4-GIF1 module coordinates organ growth and iron uptake in *Arabidopsis*. *Nature Plants*, *9*, 1318–1332. https://doi.org/10.1038/s41477-023-01475-0